

CHARACTERISTICS OF WING SECTIONS AT TRANSONIC SPEEDS

By John V. Becker

Langley Aeronautical Laboratory

INTRODUCTION

The transonic regime is presumed to begin with the first appearance of a local region of supersonic flow near the airfoil surface and to end when the flow field has become entirely supersonic. The development of theory for transonic flows has been impeded by the coexistence of subsonic and supersonic flow regions and the presence of shock. Shock boundary-layer interaction effects which exert a controlling influence in the transonic region cannot be treated by rigorous theory. The major part of existing knowledge of wing-section behavior at transonic speeds is therefore derived from experimental research, and any review of the current status such as the present one must depend largely on experimental results.

FLOW CHANGES IN THE TRANSONIC REGIME

The progressive changes in flow pattern which occur in the transonic regime are illustrated schematically in figure 1. The diagram at the upper left ($M = 0.70$) represents a condition slightly beyond the critical Mach number (M_{cr} at which sonic velocity is attained locally). A small region of supersonic flow exists, usually terminated by shock. The possibility that local supersonic flows of this type can exist without shock is a matter of considerable speculation. Theoretical studies have indicated that shock-free flows in an ideal fluid are possible in certain special cases. (See references 1 to 4, for example.) From the practical standpoint, however, the important fact is that the presence of shock does not have any seriously adverse effects on airfoil performance unless it precipitates boundary-layer separation.

As the Mach number is increased, the shock moves rearward and the local supersonic region expands rapidly. The rearward movement is analogous to shock behavior in channels, which has been treated theoretically in reference 5. Shock-stall occurs (diagram for $M = 0.90$ in fig. 1) when the adverse pressure gradient through the shock becomes large enough to precipitate separation. Considerable compression of the flow takes place ahead of the main shock (references 6 and 7) as a consequence of thickening of the boundary layer. It is important to note that shock-stall is basically a shock boundary-layer interaction phenomenon and that there is no adequate method for predicting the shock-stall Mach number. "Limiting" or "upper critical" Mach numbers predicted by theories which do not consider shock boundary-layer interaction (references 4 and 8) are at variance with experimental shock-stall Mach numbers.

Rearward movement of the shock continues at speeds beyond shock-stall. When the shock nears the trailing edge, reattachment of the flow takes place, accompanied by an increase in lift coefficient and pressure drag. The flow over the airfoil surface is now predominantly supersonic except for a region near the nose. (See diagram for $M = 0.95$ in fig. 1.)

The diagram for $M = 1.05$ in figure 1 indicates that the nature of the flow at the airfoil surface is similar to that for $M = 0.95$. A bow wave of weak intensity has appeared, marking the forward boundary of the field of influence of the airfoil but having no first-order effect on the airfoil characteristics. The transition from high subsonic to low supersonic speeds has been the subject of recent theoretical studies by Busemann and Guderley (references 9 to 12); no theoretical reasons have been found to prohibit the existence of stable flows at and near sonic velocity, and no abrupt or discontinuous changes in airfoil characteristics are anticipated in traversing sonic velocity.

As the supersonic Mach number advances, the bow wave moves closer to the airfoil nose with an attendant shrinking of the subsonic region near the nose (see diagram for $M = 1.30$ in fig. 1). For sharp-edge sections the region of subsonic flow will disappear entirely at a speed dependent on the angle through which the flow must be deviated (references 13 and 14, for example). Guderley's theoretical work (reference 10) leads to the conclusion that the process of bow-wave attachment is entirely continuous.

Force data for wings throughout the transonic range of speeds have been obtained by the "wing-flow" method both in flight (reference 15) and in the wind tunnel (reference 16). Typical data (reference 16) for a wing of aspect ratio 6.4 and NACA $65_{(112)}$-213 section are presented in figure 2. The results are considered illustrative of transonic wing-section characteristics. It is striking that all the major changes in lift, drag, and moment coefficient take place between $M = 0.75$ and 0.95; the aerodynamic center shifts from 0.25 chord at low speeds to about 0.40 chord at speeds beyond $M = 0.95$; the angle of zero lift changes from a negative low-speed value to a slightly positive value. Reattachment appears to start at $M = 0.90$, becoming complete at $M = 0.95$. These changes are in qualitative accord with theoretical requirements for transition from subsonic-type to supersonic-type flow. The wing performance at $M = 0.95$ is obviously more nearly supersonic than subsonic in character. In fact, the coefficients are in crude agreement with calculated values appropriate to $M = 1.30$, for a sharp-edge cambered wing in pure supersonic flow. It may therefore be reasoned that no first-order changes in performance will appear at speeds beyond $M \approx 0.95$.

Typical changes in pressure distribution in the transonic region are shown in figure 3 for the NACA 23012 section (references 17 and 18). Lift and drag data corresponding to the pressure distributions are given in the upper left diagram. The effect of increasing Mach number on the pressure coefficients at subcritical speeds (compare curves for $M = 0.29$

and $M = 0.59$ in fig. 3) is predictable by approximate theoretical methods. (See reference 3, for example.) The presence of supersonic flow terminated by a strong shock (but no obvious flow separation) is clearly evident in the diagram for $M = 0.74$ in figure 3. In the last diagram in figure 3, for $M = 0.88$, the shocks lie just ahead of the trailing edge. The supersonic character of the flow is illustrated by comparison of the measured pressures with those predicted by supersonic (Prandtl-Meyer) theory applied to the part of the section aft of the sonic point. The shapes of the measured and computed curves are similar although the measured suction pressures are, of course, considerably lower because the depth of the supersonic region is actually finite rather than infinite as assumed by the theory. The development of pressure drag is apparent from the progressive increase of pressure at the nose beyond M_{cr} together with the large decrease of pressure over the rear portion beyond shock-stall.

SYSTEMATIC INVESTIGATION OF SHAPE PARAMETERS AT HIGH SUBSONIC SPEEDS

Wind-tunnel investigations of a large number of related wing sections have been made at speeds up to $M = 0.94$. The succeeding discussion consists of a brief review of the effects of the more important shape parameters as determined from this research.

Thickness ratio.- The transonic characteristics of two symmetrical airfoils differing only in thickness ratio (reference 19) are shown in figure 4. The thinner airfoil has not only a higher shock-stall speed but also smaller undesirable changes in force characteristics after shock-stall. It will be noted that the critical Mach number does not coincide with the speed of shock-stall. In fact, the 6-percent-thick airfoil which has the higher force-break speed and superior supercritical characteristics has the lower critical speed. This result leads to the conclusion that the critical Mach number is useful only to denote the beginning of the transonic region; it does not coincide with the speed of force-break and is no criterion of airfoil behavior beyond the point of force-break.

The values of the drag coefficients at sonic velocity were estimated from wing-flow data (references 15 and 16), the transonic similarity rule (reference 20) being used to correct the available data to the desired thickness ratio. The drags of the two sections at $M = 1.0$ (fig. 4) are about three times and eight times the low-speed values, respectively, for the 6- and 12-percent-thick sections at these Reynolds numbers.

Figure 5 is a plot of minimum drag coefficient against thickness ratio. At subcritical speeds (curve for $M = 0.65$) the drag is not

greatly affected by thickness ratio but, beginning at a speed somewhat below shock–stall, the drag rises steeply with increasing thickness. According to the transonic similarity rule (references 20 and 21) the drag coefficient of a family of thin airfoils differing only in thickness is related to the thickness and Mach number as follows:

$$\frac{M^2 c_d}{(t/c)^{5/3}} = f\left[\frac{M-1}{(t/c)^{2/3}}\right]$$

At $M = 1$ this relation yields

$$c_{d_{M=1.0}} \propto (t/c)^{5/3}$$

Systematic drag data (fig. 5) at the highest speed for which data were obtained in reference 19 ($M = 0.94$) appear to agree with this five–thirds power rule. (The theoretical (dashed) curves of figure 5 were fitted to the test data at $\frac{t}{c} = 0.09$). For cambered sections the agreement is somewhat less satisfactory than for symmetrical sections. In purely supersonic flow the pressure drag varies approximately as the second power of the thickness ratio. Thus, the effect of thickness ratio will probably not change appreciably in the region between sonic speed and the speed at which bow–wave attachment occurs.

Camber.– Figure 6 compares the performance of two sections differing only in camber (reference 22). These sections are modified versions of the NACA four–digit series and are designed to have higher critical speeds than the four–digit series. The significance of the designation numbers can be seen from the following specifications for the cambered section 2,35,12–.55,40:

Maximum camber, percent chord	2
Position of maximum camber, percent chord	35
Maximum thickness, percent chord	12
Leading–edge radius	$0.55c\left(\frac{t}{c}\right)^2$
Position of maximum thickness, percent chord	40

The symmetrical section operating at $c_l = 0.20$ has not only higher force–break Mach numbers but also much smaller undesirable changes in angle of attack and changes in moment after force–break; the change in angle of attack, for example, is only 1.7° for the symmetrical section as compared with 4.5° for the cambered airfoil. A contributing factor to the large trim change of the cambered section is the shift in angle of zero lift inherent in the transition from subsonic–type to supersonic–type flows. (See fig. 2.)

The 0,00,12–.55,40 airfoil of figure 6 is identical with the NACA 0012–34 airfoil of figure 4 except for leading-edge radius. The results shown for the two sections were obtained at Reynolds numbers differing by a factor of about 10. Comparison of the data from the two tests indicates differences which are believed to be attributable primarily to scale effects, although the model-support methods used also differed and some uncertainty exists as to the possibility of tunnel-wall constriction effects, particularly for the 0,00,12–.55,40 data at the highest test speeds. It is important to note, however, that analysis of the data from either of these investigations (reference 19 or 22) leads to the same conclusions regarding optimum shapes.

Further insight into the effects of camber on shock-stall characteristics can be obtained by a study of typical pressure distributions such as those shown in figure 7. When operating at an appreciable lift coefficient, the thin symmetrical section has a high suction peak near the leading edge, while the cambered section chosen for comparison has a flat pressure-distribution diagram. The symmetrical section obviously has the lower critical Mach number of the two, but it is important to note that sonic velocity and shock will first occur near the nose. The cambered section, on the other hand, will develop shock on the rear of the airfoil where the boundary layer is more susceptible to separation. The high-speed lift characteristics of these two sections, which are also shown in figure 7, indicate that shock-stall occurs shortly after the formation of shock on the rear portion of the cambered airfoil. Shock develops at a lower free-stream speed on the symmetrical section but has no deleterious effects on performance until M_{cr} is exceeded by about 0.17. The critical Mach numbers in this figure were obtained from high-speed pressure-distribution data; thus, there is no question involved as to the adequacy of methods of estimating M_{cr} from low-speed data. In spite of its lower critical speed, the symmetrical section has a higher lift-break Mach number than the cambered section for either of the two angles of attack shown in figure 7.

Substantiation of this line of reasoning is obtained from schlieren flow photographs for these two airfoils obtained in the Langley rectangular high-speed tunnel. Figure 8 for the symmetrical section indicates that the main shock is still near the leading edge, even though the critical Mach number has been exceeded by 0.10. There is no evidence of flow separation; measurement of the wake width at the trailing edge indicates the same value as was found for $M = 0.30$. The schlieren photograph for the cambered section (fig. 9) indicates the occurrence of shock just ahead of the trailing edge and the presence of flow separation at a Mach number only 0.05 above the critical. The flow separation was actually observed to start at a Mach number about 0.02 above the critical value. An analysis of the schlieren diagrams of figures 8 and 9 is made in figure 10. A maximum local Mach number of 1.20 was measured for the symmetrical section as compared with 1.11 for the cambered section. It would, therefore, be expected that the shock at the nose of the symmetrical section is considerably more intense than the shock for the cambered section. This difference in shock strength is probably accentuated by the

fact that the boundary layer thickens extensively ahead of the main shock on the cambered airfoil, thereby reducing the local Mach number to a value close to unity just ahead of the shock (reference 23). Flow separation is thus precipitated by a very weak shock when the shock occurs near the rear of the airfoil. This explains the behavior of high-critical-speed and low-drag types of airfoils when operating at lift coefficients near their design values (references 24 to 26). Figure 11 shows the force-break characteristics of the NACA 66-210 airfoil (reference 26) as an example. In the vicinity of design lift the force-breaks occur shortly after the first appearance of shock at M_{cr}. At lift coefficients appreciably higher or lower than the design value, high suction pressure peaks develop at the airfoil nose but the existence of shock in this position does not cause force-break, and the critical Mach number is exceeded by a wide margin before the occurrence of force-break.

A photograph of the flow taken near the Mach number of force-break of the symmetrical NACA 0009-64 section is shown in figure 12. The main shock has moved from the vicinity of the nose to the 0.45-chord position, where it causes an appreciable disturbance of the boundary layer but no extensive flow separation. An analysis of this photograph and comparison with the cambered section is made in figure 13 in which both sections are operating at the same speed, the same geometric angle of attack, and approximately the same lift coefficient prior to force-break. The cambered section again has a weak shock preceded by a maximum Mach number close to unity. As in the previous illustration, appreciable flow separation and force-break have occurred, although the critical Mach number has been exceeded only by 0.05. The symmetrical section, on the other hand, carries a relatively strong shock of about equal depth normal to the airfoil without any evidence of shock stall. The shock losses for the symmetrical section will obviously be high, but no appreciable separation losses are present. The cambered section on the other hand encounters no appreciable shock loss but has a high separation loss. It is therefore difficult to determine from this analysis the relative lift-drag values of the two sections and this question must be answered by force data. An analysis of typical force-test results for related airfoils of varying camber (reference 22) is shown in figure 14. The camber in percent of chord which resulted in the maximum lift-drag ratio is plotted against Mach number for various operating lift coefficients. At low speed appreciable camber is desirable, but the optimum camber is seen to decrease as the Mach number increases. When the critical Mach number is exceeded, the optimum amount of camber drops rapidly to zero. For the 12-percent-thick sections used in the illustration, the symmetrical section has the best lift-drag ratios at all Mach numbers beyond 0.76 for all the lift coefficients tested. An NACA investigation of 16-series sections of various camber (reference 24) revealed a similar trend of decreasing optimum camber with increasing Mach number. Previous discussion of figure 6 revealed that symmetrical sections are desirable for transonic applications from consideration of trim and moment changes as well as from consideration of best lift-drag ratio.

Trailing-edge angle.- Virtually no information is available showing the effect of trailing-edge angle as an isolated variable. If the angle is large, the flow is subject to separation at transonic speeds which results in high drag, low lift-curve slope, and poor control-surface effectiveness (references 27 to 29). The maximum recommended values for trailing-edge angle lie in the range of 10° to 15°; smaller values are preferable.

Positions of maximum thickness.- Test data bearing on the optimum position of maximum thickness for symmetrical sections are given in references 19 and 30. The best location appears to lie between 0.4 chord and 0.5 chord.

Leading-edge radius.- At lift coefficients near zero (say, less than 0.1) the value of the leading-edge radius is not critical for symmetrical sections at high subsonic speeds (reference 31). At higher lifts the best lift-drag ratio is obtained with a leading-edge radius of about one-half the value used in the NACA four-digit series. The radii used on the NACA 16-series and 6-series airfoils are near the optimum value. The leading edge should be sharp in supersonic flow if the speed is high enough to permit bow-wave attachment (reference 32), in order to avoid the relatively high shock losses occurring near the apex of a detached bow wave. If, however, the supersonic Mach number is so low that an attached shock is not possible even if the leading edge is sharp (reference 14), then there is no reason to believe that sections having a small leading-edge radius will have inferior characteristics to comparable sharp-edge sections.

The behavior of sharp-edge supersonic-type sections has been the subject of a recent investigation at high subsonic speeds (reference 33). An unexpected phenomenon was discovered which is illustrated in figures 15 and 16. At all speeds up to $M = 0.75$ the anticipated extensive region of separated flow starting at the sharp leading edge was present as depicted in figure 15. Local supersonic velocities terminated by shock are present over the forward part of the section outside of the region of flow separation. The separated flow vanished abruptly when the Mach number was increased by 0.02 to $M = 0.77$ (fig. 16). The ability of the flow to negotiate the sharp edge is explained by the fact that the local velocity field in the vicinity of the leading edge is supersonic (reference 34). A small bubble of separation is present immediately behind the corner. In expanding about this bubble the flow is directed towards the surface, giving rise to the oblique compression shock. The origin of the foremost oblique disturbance apparent in figure 16 is uncertain. It is believed, however, that since the disturbance disappears at some distance above the airfoil it does not have any major effect on the reattachment phenomenon.

This reattachment of the flow is accompanied by an increase in lift and, in a majority of cases, little change in drag. The increased pressure drag after attachment tends to offset the reduction of separation

losses. It is important to note that, although the lift–drag ratio is increased by this phenomenon, the lift–drag ratios reached are not as high as are obtainable with round–edge sections at the same speeds (reference 33).

OPTIMUM SHAPES FOR LOW SUPERSONIC SPEED RANGE

The high–subsonic test data utilized in the foregoing discussion point towards an optimum section shape for the high–subsonic speed range which has no camber, a maximum–thickness position near the midchord point, as small values as possible of the thickness and trailing–edge angle, and a small but finite leading–edge radius. With the exception of the leading–edge radius, these specifications closely approach the theoretical requirements for an optimum section in purely supersonic flow at low supersonic speeds. There is little reason to suspect that a sharp leading edge would prove more desirable than a small rounded edge in the transonic speed range where a detached bow wave would occur with either shape. It may be conjectured, therefore, that the airfoil shape which is optimum for high–subsonic speeds will also have the best characteristics in the supersonic part of the transonic regime. It is obvious, however, that further research is needed to establish the details of airfoil performance at low supersonic speeds.

PROFILES SUITABLE FOR TRANSONIC APPLICATIONS

The following symmetrical profiles meet the approximate specifications for optimum shape discussed in the preceding sections of this paper:

NACA 0009–44	(see reference 35)
NACA 65–009	(see reference 36)
NACA 65A–009	(see reference 37)

The latter two sections could be made thicker than 9 percent without exceeding the arbitrary limit imposed on the trailing–edge angle (15°). The use of thicker sections, however, is usually prohibitive for transonic applications from consideration of power requirements as well as adverse trim and moment changes. Obviously, thinner sections having the same thickness distribution as the above profiles will also meet the approximate optimum shape requirements.

REFERENCES

1. Taylor, G. I.: The Flow of Air at High Speeds past Curved Surfaces. R. & M. No. 1381, British A.R.C., 1930.

2. Ringleb, Friedrich: Exakte Lösungen der Differentialgleichungen einer adiabatischen Gasströmung. Z.f.a.M.M., Bd. 20, Heft. 4, Aug. 1940, pp. 185–198.

3. Von Kármán, Th.: Compressibility Effects in Aerodynamics. Jour. Aero. Sci., vol. 8, no. 9, July 1941, pp. 337–356.

4. Kaplan, Carl: The Flow of a Compressible Fluid past a Curved Surface. NACA Rep. No. 768, 1943.

5. Stodola, A.: Steam and Gas Turbines. Vol. I. McGraw-Hill Book Co., Inc., 1927.

6. Ackeret, J., Feldmann, F., and Rott, N.: Investigations of Compression Shocks and Boundary Layers in Gases Moving at High Speed. NACA TM No. 1113, 1947.

7. Liepmann, Hans Wolfgang: The Interaction between Boundary Layer and Shock Waves in Transonic Flow. Jour. Aero. Sci., vol. 13, no. 12, Dec. 1946, pp. 623–638.

8. Greene, Leonard Michael: The Attenuation Method for Compressible Flow Systems. Jour. Aero. Sci., vol. 12, no. 3, July 1945, pp. 329–338.

9. Busemann, A., and Guderley, G.: The Problem of Drag at High Subsonic Speeds. Reps. and Translations No. 184, British M.O.S.(A) Völkenrode, March 1947. (Wright Field translation F-TS-3492-RE in preparation.)

10. Guderley, G.: Considerations of the Structure of Mixed Subsonic–Supersonic Flow Patterns. Tech. Rep. No. F-TR-2168-ND, Air Materiel Command (Wright Field), Oct. 1947.

11. Guderley, G.: On the Transition from a Transonic Potential Flow to a Flow with Shocks. Tech. Rep. No. F-TR-2160-ND, Air Materiel Command (Wright Field), Aug. 1947.

12. Guderley, G.: Singularities at the Sonic Velocity. Tech. Rep. No. F-TR-1171-ND, Air Materiel Command (Wright Field), Nov. 1947. (Preprint.)

13. Crocco, Luigi: Singolarità della corrente gassosa imperacustica nell'intorno di una prora a diedro. L'Aerotecnica, vol. XVII, fasc. 6, June 1937, pp. 519–534.

14. Burcher, Marie A.: Compressible Flow Tables for Air. NACA TN No. 1592, 1948.

15. Gilruth, R. R., and Wetmore, J. W.: Preliminary Tests of Several Airfoil Models in the Transonic Speed Range. NACA ACR No. L5E08, 1945.

16. Weaver, John H.: A Method of Wind–Tunnel Testing through the Transonic Range. Jour. Aero. Sci., vol. 15, no. 1, Jan. 1948, pp. 28–34.

17. Göthert, B.: Druckverteilungsschaubilder für das Profil NACA 230–12 bei hohen Unterschallgeschwindigkeiten. UM Nr. 1260/2, Deutsche Luftfahrtforschung (Berlin–Adlershof), 1944.

18. Göthert, B.: Hochgeschwindigkeitsmessungen an Profilen der Reihe NACA 230 mit verschiedenen Dickenverhältnissen. UM Nr. 1259/2, Deutsche Luftfahrtforschung (Berlin–Adlershof), 1944.

19. Ferri, Antonio: Completed Tabulation in the United States of Tests of 24 Airfoils at High Mach Numbers (Derived from Interrupted Work at Guidonia, Italy, in the 1.31– by 1.74–Foot High–Speed Tunnel). NACA ACR No. L5E21, 1945.

20. Von Kármán, Theodore: The Similarity Law of Transonic Flow. Jour. Math. and Phys., vol. XXVI, no. 3, Oct. 1947, pp. 182–190.

21. Kaplan, Carl: On Similarity Rules for Transonic Flow. NACA TN No. 1527, 1948.

22. Göthert, B.: Hochgeschwindigkeitsmessungen an Profilen gleicher Dickenverteilung mit verschiedener Krümmung im DVL–Hochgeschwindigkeitswindkanal (2.7m Durchm.) FB Nr. 1910, Deutsche Luftfahrtforschung (Berlin–Adlershof), 1944.

23. Stack, John: Compressible Flows in Aeronautics. Jour. Aero. Sci., vol. 12, no. 2, April 1945, pp. 127–143.

24. Lindsey, W. F., Stevenson, D. B., and Daley, Bernard N.: Aerodynamic Characteristics of 24 NACA 16–Series Airfoils at Mach Numbers between 0.3 and 0.8. NACA TN No. 1546, 1948.

25. Anderson, Joseph L.: Tests of NACA 65(216)–420 and 66(218)–420 Airfoils at High Speeds. NACA MR, April 1944.

26. Graham, Donald J.: High-Speed Tests of an Airfoil Section Cambered to Have Critical Mach Numbers Higher Than Those Attainable with a Uniform-Load Mean Line. NACA TN No. 1396, 1947.

27. Stevenson, David B., and Bryne, Robert W.: High-Speed Wind-Tunnel Tests of an NACA 16-009 Airfoil Having a 32.9-Percent-Chord Flap with an Overhang of 20.7 Percent of the Flap Chord. NACA TN No. 1406, 1947.

28. Stevenson, David B., and Adler, Alfred A.: High-Speed Wind-Tunnel Tests of an NACA 0009-64 Airfoil Having a 33.4-Percent-Chord Flap with an Overhang 20.1 Percent of the Flap Chord. NACA TN No. 1417, 1947.

29. Lindsey, W. F.: Effect of Compressibility on the Pressures and Forces Acting on a Modified NACA 65,3-019 Airfoil Having a 0.20-Chord Flap. NACA ACR No. L5G31a, 1946.

30. Göthert, B.: Hochgeschwindigkeits-Untersuchungen an symmetrischen Profilen mit verschiedenen Dickenverhältnissen im DVL-Hochgeschwindigkeitswindkanal (2.7m Durchm.) und Vergleich mit Messungen in anderen Windkanälen. FB Nr. 1506, Deutsche Luftfahrtforschung (Berlin-Adlershof), 1941.

31. Göthert, B.: Widerstandsanstieg bei Profilen im Bereich hoher Unterschallgeschwindigkeiten. Tech. Berichte, Bd. II, Teil 7, 1944.

32. Busemann, A., and Walchner, O.: Profileigenschaften bei Überschallgeschwindigkeit. Forsch. auf dem Geb. des Ingenieurw. Ausg. A; Bd. 4, Heft 2, March/April 1933, pp. 87-92.

33. Lindsey, W. F., Daley, Bernard N., and Humphreys, Milton D.: The Flow and Force Characteristics of Supersonic Airfoils at High Subsonic Speeds. NACA TN No. 1211, 1947.

34. Stack, John: Shock Stalled Flows for Supersonic Type Airfoils at Transonic Speeds. Paper presented at 6th Int. Cong. Appl. Mech. (Paris), Sept. 22-29, 1946.

35. Stack, John, and Von Doenhoff, Albert E.: Tests of 16 Related Airfoils at High Speeds. NACA Rep. No. 492, 1934.

36. Abbott, Ira H., Von Doenhoff, Albert E., and Stivers, Louis S., Jr.: Summary of Airfoil Data. NACA Rep. No. 824, 1945.

37. Loftin, Laurence K., Jr.: Theoretical and Experimental Data for NACA 6A-Series Airfoil Sections. NACA TN No. 1368, 1947.

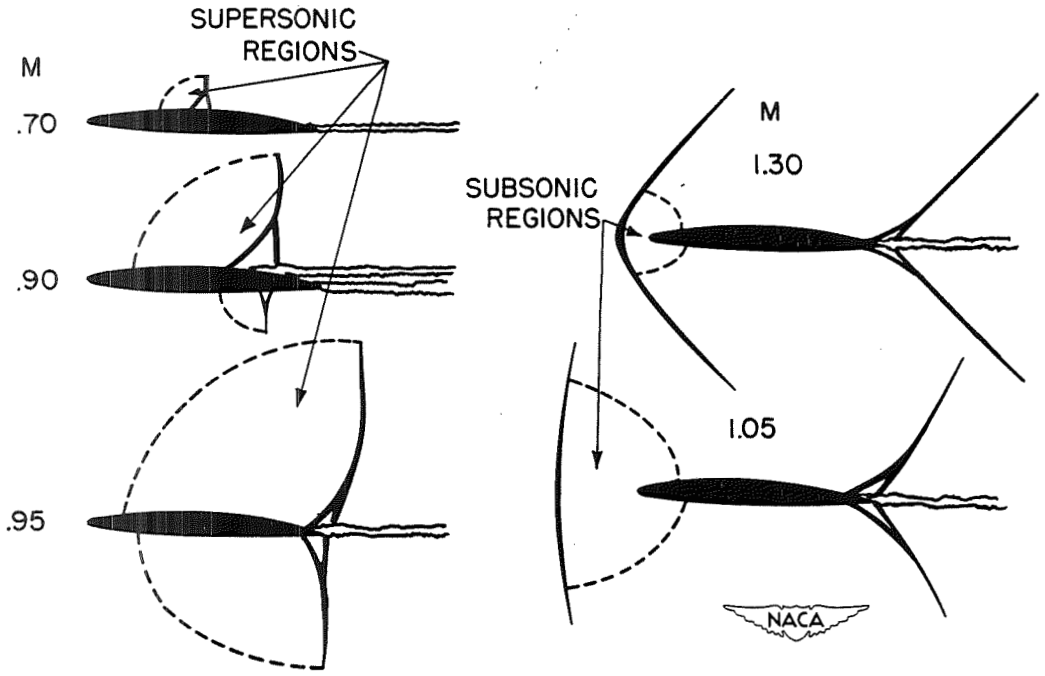

Figure 1.- Transonic flow patterns.

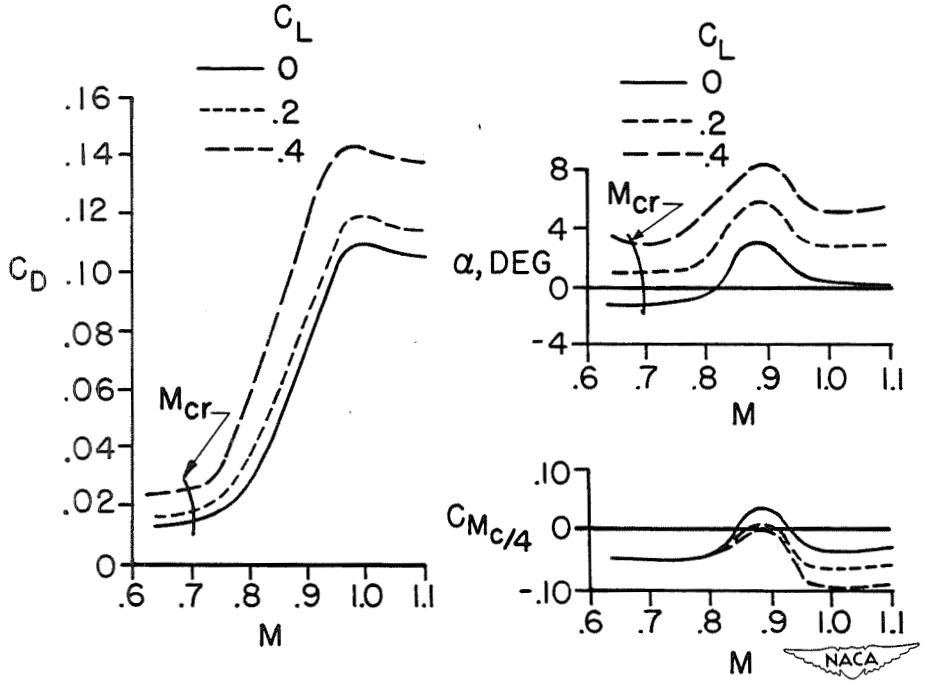

Figure 2.- Transonic force data for a typical wing. NACA $65_{(112)}$-213, a = 0.5 airfoil; aspect ratio, 6.4.

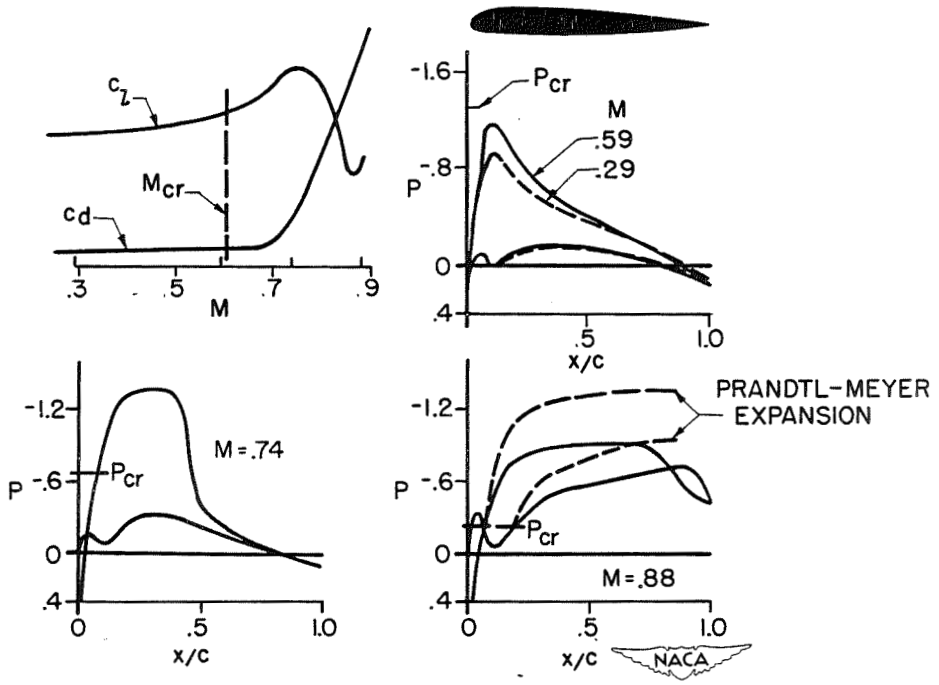

Figure 3.- Typical pressure-distribution data. NACA 23012 airfoil; $\alpha = 1.6^{\circ}$.

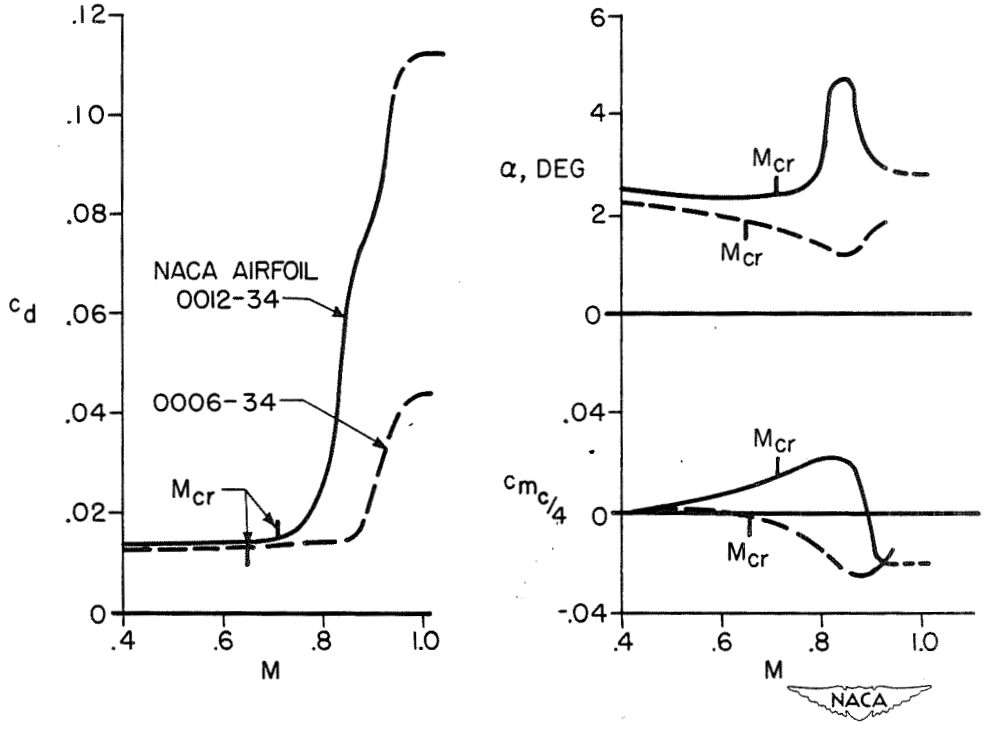

Figure 4.- Effects of thickness ratio. $c_l = 0.20$; $R \approx 0.4 \times 10^6$.

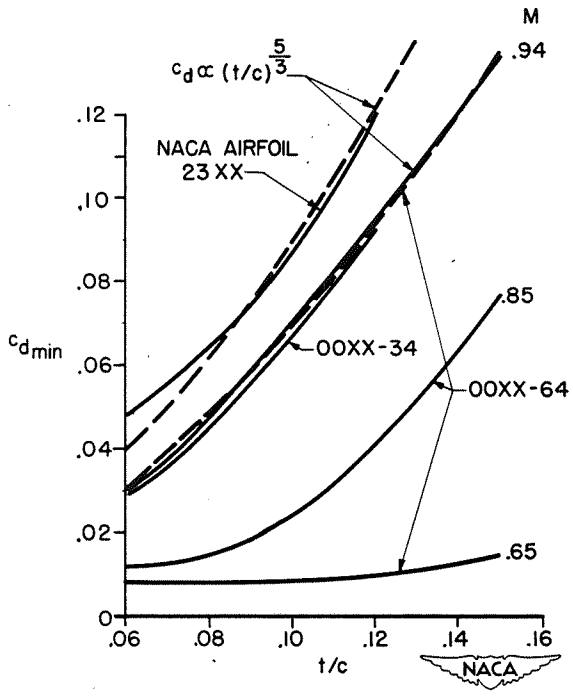

Figure 5.- Effect of thickness ratio on minimum drag.

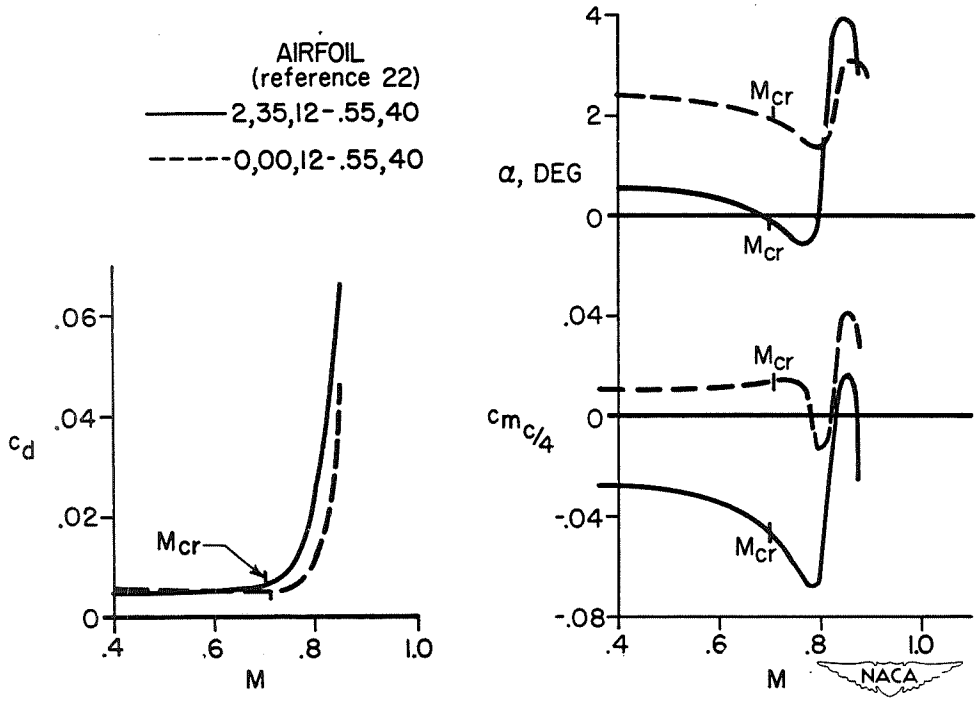

Figure 6.- Effects of camber. $c_l = 0.20$; $R \approx 4 \times 10^6$.

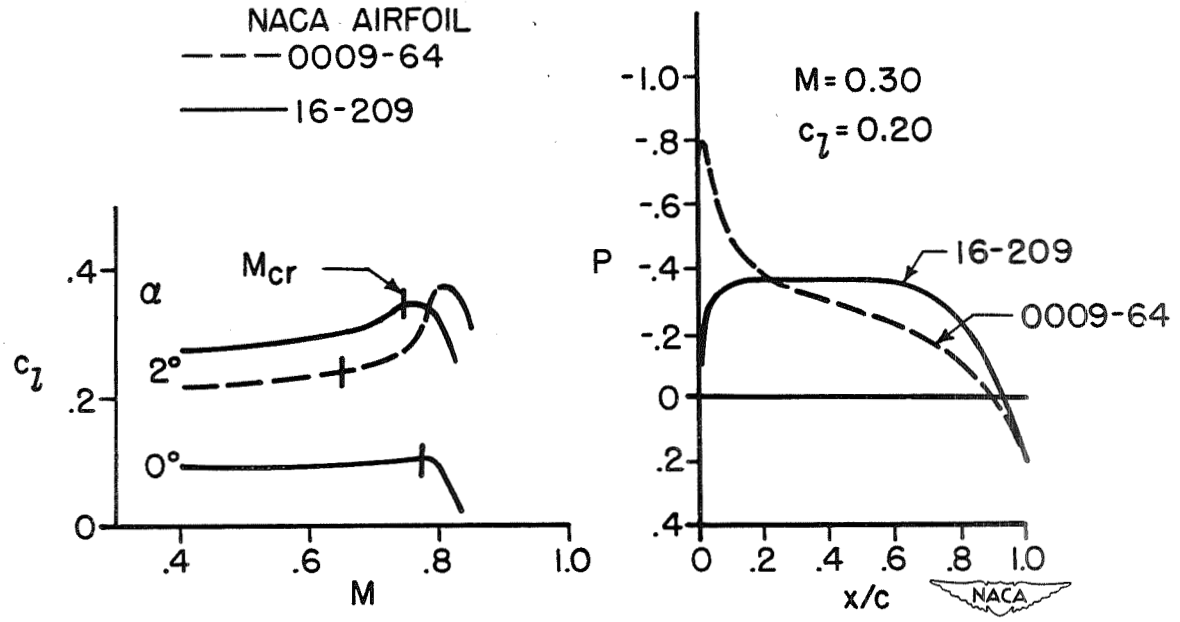

Figure 7.- Effects of camber on lift and upper-surface pressure-distribution characteristics of thin sections.

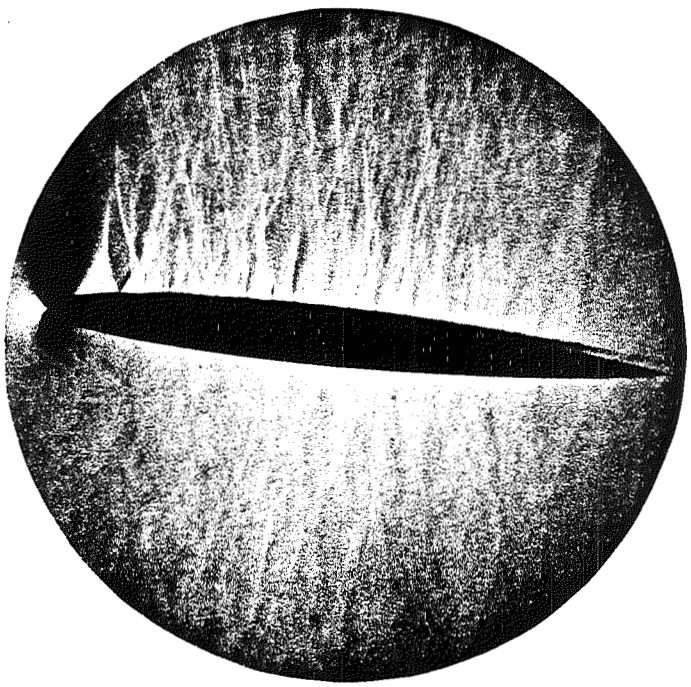

Figure 8.- Schlieren flow photograph of NACA 0009-64 airfoil. $\alpha = 2^{\circ}$; $M = 0.75 = M_{cr} + 0.10$.

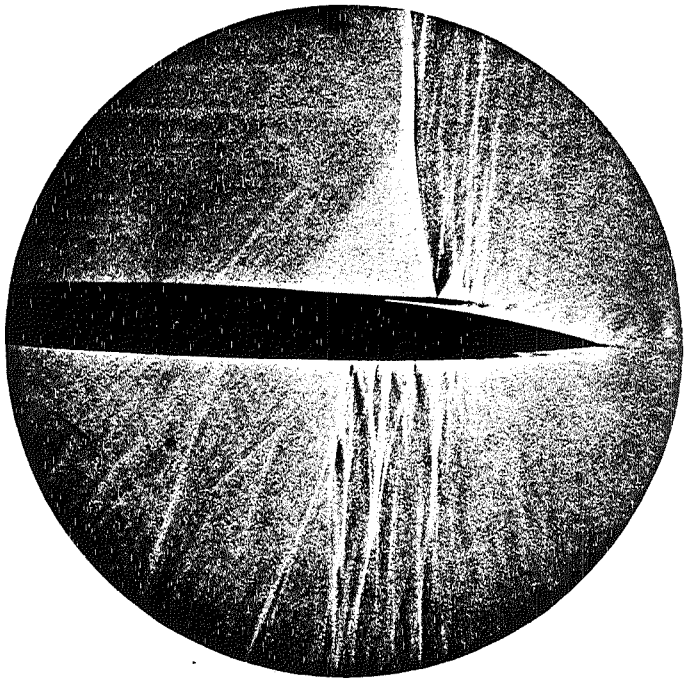

NACA

Figure 9.- Schlieren flow photograph of NACA 16-209 airfoil. $\alpha = 0^{\circ}$; $M = 0.83 = M_{cr} + 0.05$.

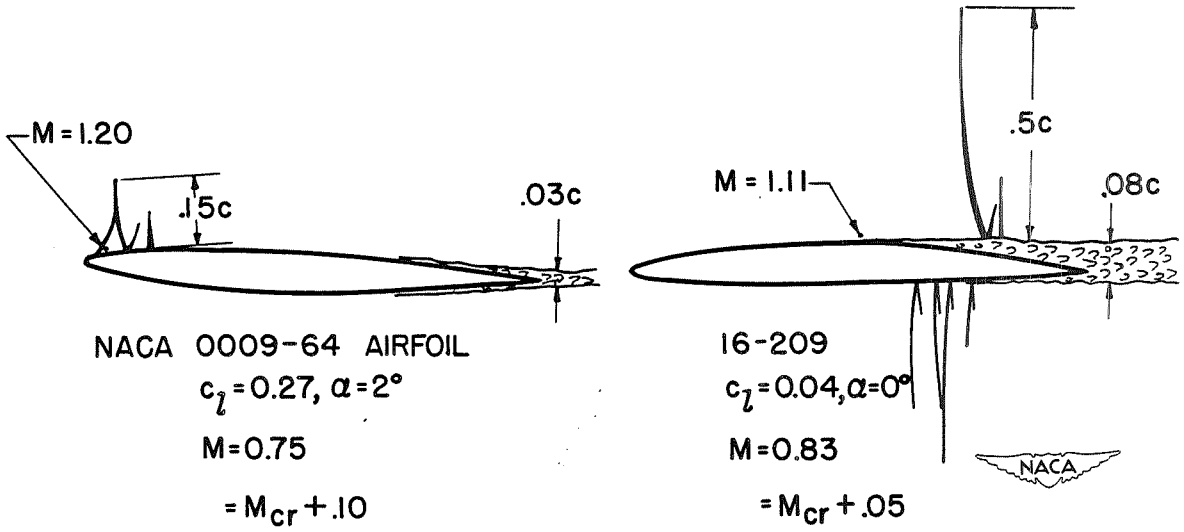

Figure 10.- Analysis of flow photographs (figs. 8 and 9).

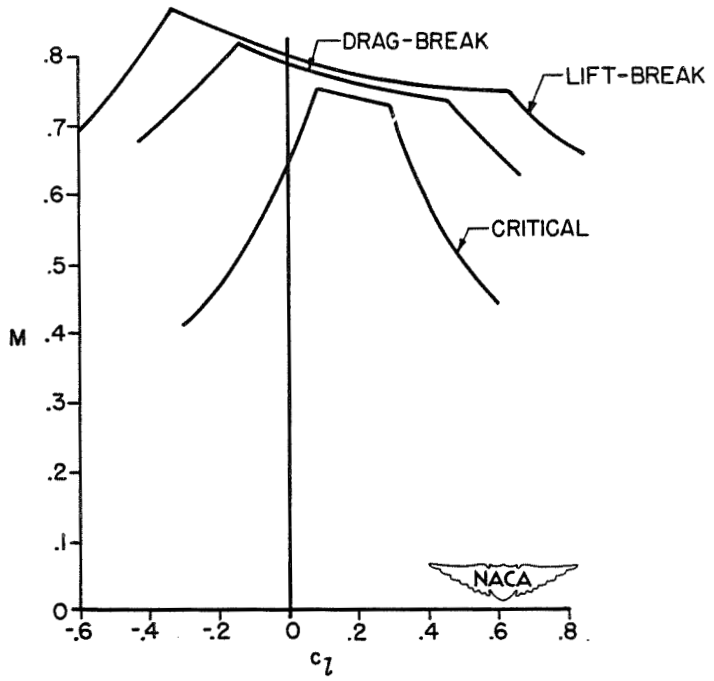

Figure 11.- Critical and force-break Mach numbers for an NACA 66-210 airfoil.

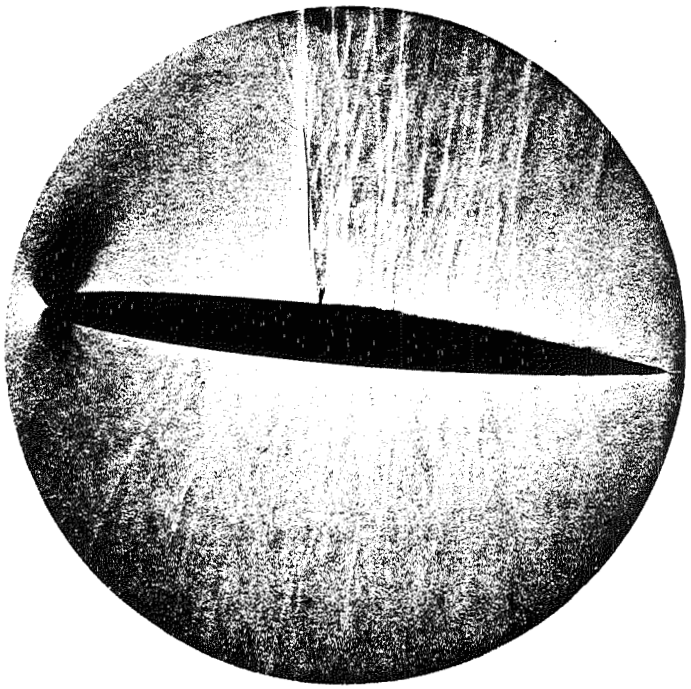

Figure 12.- Schlieren flow photograph of NACA 0009-64 airfoil. $\alpha = 2^{\circ}$; $M = 0.80 = M_{cr} + 0.15$.